Computer simulation of SIA migration in bcc and hcp metals

R.C. Pasianot[a,b,*], A.M. Monti[a], G. Simonelli[c], E.J. Savino[a]

[a] *Dpto. Materiales, CNEA, Avda. Libertador 8250, 1429 Buenos Aires, Argentina*
[b] *CONICET, Av. Rivadavia 1917, 1033 Buenos Aires, Argentina*
[c] *Instituto de Física, Univ. Nac. de Tucumán, Av. Independencia 1800, 4000 S.M. de Tucumán, Argentina*

Abstract

A Molecular statics and dynamics study of self-interstitial diffusion mechanisms in model Fe, Mo (bcc) and Zr (hcp) is performed. Embedded-atom-method type interatomic potentials developed by the present authors are employed. Molecular dynamics simulations are carried out at constant energy and volume for different temperatures. Defect diffusion coefficients are computed and the migration jumps at both, low and relatively high temperatures, are qualitatively identified by simple visualization techniques. The relevance of crowdion-type interstitials is demonstrated in both hcp and bcc structures. Highly non-Arrhenius behavior is predicted for the basal diffusion in Zr. Also, the dynamically computed migration energies result roughly in half of the values computed using static techniques. This points to the difficulties of a straight application of Transition State Theory under conditions of moderately complex defect and/or energy barrier structures. © 2000 Elsevier Science B.V. All rights reserved.

PACS: 61.72.-y; 61.72.Ji; 66.30.Fq

1. Introduction

Recent computer simulation studies of defect structure on bcc [1,2] and hcp [3,4] metals based on Embedded-atom-method (EAM) type interatomic potentials have obtained self-interstitial (SIA) configurations that undergo one-dimensional (1D) migration, either individually or as small clusters. There is, however, no systematic understanding on how this migration mechanism arises or of the model features responsible for such behavior. Particularly, in the bcc case, very low migration energies have been computed by molecular dynamics (MD) [2], though no notice has been given to the fact that those values are at variance with the substantially higher energy barriers predicted by molecular statics (MS), which in turn constitute basic ingredients of the transition state formalism [5] for obtaining jump frequencies.

In the present work we study the SIA migration in EAM models for Fe, Mo (bcc) and Zr (hcp) by MS and MD. It is shown, by comparing the results from both techniques, that a consistent picture emerges able to shed some light on the questions posed above.

2. Method

The potentials details can be found in [3,6] for Zr and Fe, respectively. The Mo potential is built on the same lines as for Fe and has been used before to study phonon spectra [7]. Briefly, they are fitted to the cohesive energy, lattice parameter(s), elastic constants and vacancy formation energy. Also, interstitial relaxation volumes close to experimental values [8–10] are obtained. We believe the latter is a particularly relevant feature to the present investigation. Simulation crystallites are either approximately cubic with periodic boundaries (MD) or spherical with fixed boundaries (MS) and contain at least 2000 moving atoms.

2.1. MS simulations

A variant of the DEVIL code [11] is used to find configurational energy extrema of the defective lattice. In order to asses stability and identify possible reaction paths, the vibrational spectra of about 150 coupled atoms taken from these structures are then computed

---

* Corresponding author.
E-mail address: pasianot@cnea.gov.ar (R.C. Pasianot).

through diagonalization of the respective force constants matrices. Also, the energy barrier for the (proposed) migration path joining two such configurations, i and f, is calculated by linear interpolation between the corresponding 3N-dimensional coordinates of the crystallite, R_i and R_f,

$$R(\alpha) = (1 - \alpha)R_i + \alpha R_f$$

and relaxation of the system energy restricted to the hyperplane perpendicular to $(R_f - R_i)$ for each given value of α [12]. This is easily achieved by subtracting to the 3N-dimensional force of the conjugate gradient method [13] (on which DEVIL is based) its component along that direction. Such a detailed analysis is needed only for the bcc structures, where several migration mechanisms compete, and are very close in energy as explained later on.

2.2. MD simulations

A modified version of the DYNAMO code [14] is employed. The system is first run for some time under temperature control and zero pressure (N, $P = 0$, T) for equilibration purposes. Conditions are then switched to the microcanonical ensemble (N, E, V) in order to study the migration dynamics. The latter is followed by at least 600 ps, and the lowest temperatures studied are such that diffusion is just revealed for those simulation times. Crystallite configurations are output each 0.5 ps, and in a later stage, the whole set of them is searched for the interstitials. These are considered to be the atoms beyond a given distance from any perfect lattice node, averaging their coordinates if more than one is found. The procedure is also checked using simple visual methods. In this way the defect trajectory is reconstructed. A point to note here is that different ensemble conditions produce different defect trajectories, and in the low T range studied, this may have a significant effect on the computed diffusion coefficient (high T's were not checked for such an effect). (N, E, V) conditions are therefore selected because they are the closest to true Newtonian dynamics.

To obtain the diffusion coefficient D, the total run time is partitioned in intervals of equal duration τ, and within each of them, interstitial positions are selected at time intervals $\Delta\tau$. The latter is chosen such as to approach conditions for time non-correlation between configurations. A statistical analysis performed on the resulting data set allows one to compute D according to

$$D_{\alpha\alpha} = \frac{1}{2} \frac{\langle x_\alpha x_\alpha \rangle_\tau}{\tau},$$

where x_α stands for component α of the defect displacement. In order to assure consistency of the procedure, τ is generally varied between 5 and 50 ps until the

quotient above is almost constant. Migration energies and pre-exponential factors are obtained from the Ds so computed for several temperatures by the standard procedure of Arrhenius plots. The whole method is no more than a straight application of random walk theory and essentially coincides with that already employed in Ref. [15].

3. Results

3.1. hcp Zr

MS simulations on the Zr lattice using several selected EAM potentials [3] predict either the basal crowdion, BC or basal dumbbell, BS, as the stable SIA configurations. Unfortunately, experimental evidences in the low temperature region are not conclusive on this point [3]. Both configurations extend along the $\langle 11\bar{2}0 \rangle$ atomic rows and result very close in energy among each other (≈ 0.01 eV), facts that point to the ease of 1D migration. Also, for our specific potential, all the other common configurations lie at least 0.3 eV above in energy, except for the basal octahedral, BO, which is 0.13 eV higher. Moreover, all of them are unstable, which means that one or more frequencies of the corresponding vibrational spectra are imaginary.

The MD simulations are consistent with the above at low temperature. However, as the latter increases, two qualitatively different behaviors occur, on the basal plane and along the c axis, respectively. Fig. 1 shows the Arrhenius plot for the basal diffusion coefficient $D_a = (D_{xx} + D_{yy})/2$. For the low T region it is seen that D_a increases with T, while the interstitial performs a back-and-forth movement confined to a single $\langle 1\,1\,\bar{2}\,0 \rangle$ atomic row. A strong decrease is evidenced at about 200 K simultaneous with the beginning of interstitial exchange among different $\langle 1\,1\,\bar{2}\,0 \rangle$ rows. This phenomenom can be understood as a defocusing effect of vibrations perpendicular to the compact rows. A rise follows again, and finally saturation is obtained at
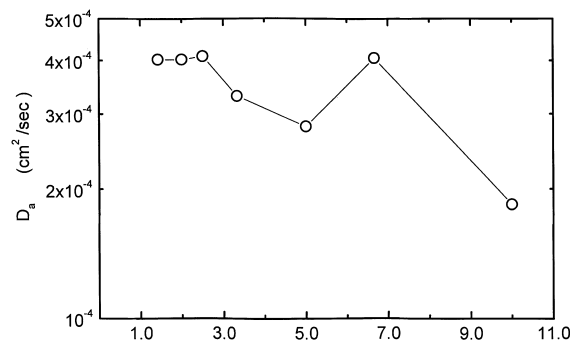

Fig. 1. Zr SIA diffusion coefficient on the basal plane, D_a.

higher temperatures as if the process were no longer thermally activated.

3D motion is already present at 300 K with some few jumps along the c axis within the 600 ps of the run. In contrast with the above, D_c shows a normal Arrhenius behavior with an activation energy $E_m \approx 0.14$ eV, and a ratio $D_c/D_a \approx 0.5$ for the highest temperature studied (700 K). Note this E_m value is about half the expected 0.3 eV from static calculations. Other authors [16] have obtained the same transition from 1D up to 3D motion with temperature increase, even within similar temperature intervals. They used, however, a different EAM potential [17] and a method based on the computation of defect jump frequencies.

3.2. bcc Fe and Mo

For both metals MS simulations predict, consistent with experiments [18], the $\langle 110 \rangle$ dumbbell as the stable SIA [12]. This configuration is followed in energy by the $\langle 111 \rangle$ crowdion, with all the other standard ones unstable. As in the above, the $\langle 111 \rangle$ rows play now the role of flat energy pathways. The energy difference between the crowdion and the (unstable) $\langle 111 \rangle$ dumbbell, amounts to just some hundredths of eV for both metals.

Several jumps may be proposed for the $\langle 110 \rangle$ dumbbell: on-site rotation (R) leading to no migration at all, and jumps to nearest (single 'S') or further (double 'D', triple 'T', etc.) $\langle 111 \rangle$ neighbors. In turn, these jumps can be acomplished with or without simultaneous dumbbell rotation. As an instance of notation, the symbol DR stands for a jump to 2nd neighbors with simultaneous dumbbell rotation, and so on. Besides, there exists also the possibility of conversion to the metastable crowdion. The energy barriers for the most relevant jumps to our discussion are gathered in Fig. 2 for Fe; similar shapes are obtained for Mo. Quantitative differences appear, however, among our two bcc models. In Fe the SR process is the least energy one though all E_ms fall within a narrow range, some 0.01 eV, with respect to the representative value ≈ 0.3 eV. For Mo the SR jump is also the favored one with $E_m(SR) \approx 0.6$ eV, closely followed by R, being any other jump at least 0.1 eV higher in energy.

These differences are recognized in the MD runs at low T. Fig. 3 for Fe, shows the defect coordinates (X, Y, Z) as a function of time computed at 320 K. No process is favored and even triple jumps are already present. On the other hand, a similar plot for Mo at 750 K, Fig. 4, shows an overwhelming number of SR and a few R and S processes but no multiple jumps. The vertical noise seen as bands in those graphs is introduced by the defect search method, which switches between locating the dumbbell center or only one atom. This is however a useful feature because it allows one to identify the dumbbell orientation, indicated in the bottom part
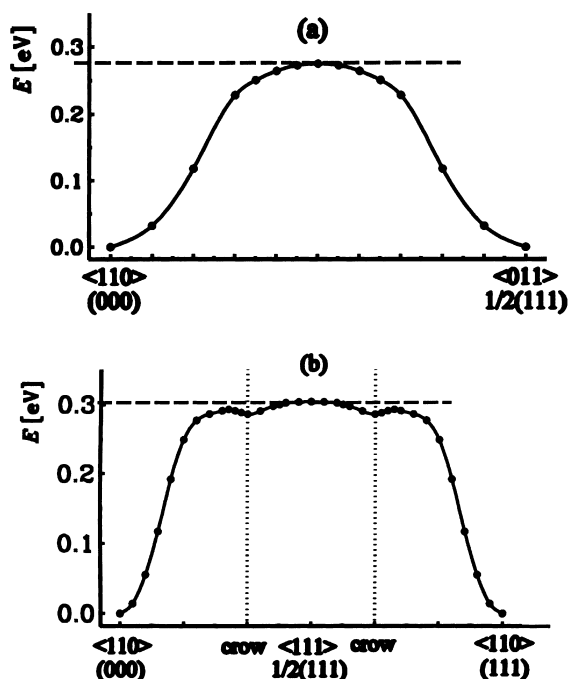
Fig. 2. SIA migration energy barriers in bcc Fe. (a) jump to n.n. with rotation, (b) id. to second $\langle 1\,1\,1 \rangle$ neighbor, no rotation.

of the figures: notice that the bands appear associated with pairs of cartesian coordinates at a time. Besides, the jump length is calculated from the trajectory steps.

The weight of multiple or non-SR jumps increases with further rise in T; an instance of this is Fig. 5, where a 3D view of the interstitial path for Fe at 700 K is shown. A similar though less pronounced effect is obtained for Mo. Indicated on the figure are the total run time, the time step between points (configurations) and

Fig. 3. SIA trajectory in Fe at 320 K computed by MD.

Fig. 4. SIA trajectory in Mo at 750 K computed by MD.

Fig. 6. Arrhenius plots for SIA migration in Fe and Mo.

Fig. 5. 3D view of SIA trajectory in Fe at 700 K.

Fig. 7. Dumbbell orientations for Fe at 1000 K.

the nearest neighbor distance (minimum jump length). When activation energies are computed from trajectories obtained for various T, see Fig. 6 for the Arrhenius plots, $E_m \approx 0.13$ eV and $\ap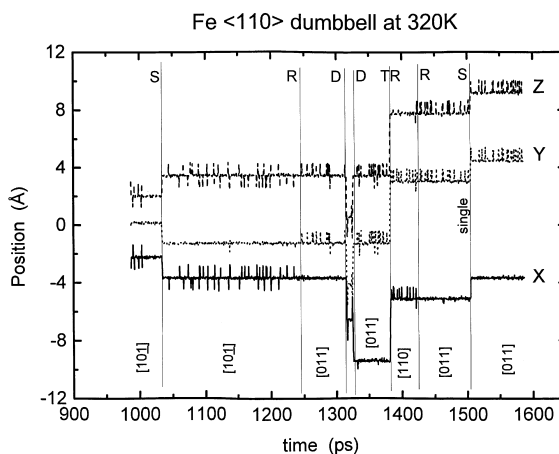prox 0.48$ eV for Fe and Mo, respectively result. These values are much lower than the static 0.3 and 0.6 eV quoted before.

4. Discussion and conclusions

There are several points of interest to mention. First, and acknowledging that it is not the purpose of the present work, the values of the migration energies obtained do not necessarily agree with experimental findings. Representative measured E_m values are 0.3, 0.3 and 0.08 eV for Zr, Fe and Mo, respectively

[18]. Particularly, all bcc transition metals but Fe show very low SIA migration energies, and to the authors knowledge, no interatomic potential has yet been able to reproduce such low values [19]. This seems to be a fundamental issue that remains open.

Second, the differences between static and dynamic activation energies can be explained if the temperature effect is to increase the time spent in crowdion-like configurations relative to the minimum energy one. The low temperature picture of a system jumping between well defined potential minima, e.g., Figs. 3 and 4, does not hold as the temperature is raised and wider regions of phase space become accessible. Though in a much more complicated context than the present one, we believe this is related to the concept of changing energy landscapes with temperature that appears in glass forming liquids dynamics [20]. To better substantiate these arguments, Fig. 7 shows the dumbbell orientations for Fe at 1000 K viewed in the standard cubic stereographic triangle. SIA populations are assigned the labels $\langle 100 \rangle$, $\langle 110 \rangle$ and $\langle 111 \rangle$ according to the maximum

projection of the dumbbell axis; the figure represents a distribution of 13%, 41% and 43%, respectively. A similar analysis for Mo at 1400 K produces 12%, 62% and 26%, i.e., large contributions of configurations different from $\langle 110 \rangle$ in both cases. Apparently at variance with the present results, good agreement between static and dynamic migration energies was found in an early study of SIA migration in W [15] using a pair potential. A possible explanation refers to the rather different structure there reported for the jump saddle point configuration, that seems to be geometrically unrelated to crowdion-like configurations. This fact is also reflected by the relatively wide energy separation between the two configurations, 0.38 eV and 0.95 eV, respectively, found by those authors.

Finally, it is seen that computed static and dynamic E_m values are in better agreement for Mo than for Fe. This is in line with the expectation from the previous paragraph, that the effects there described should become more relevant the lower the migration energies involved and the richer the structure of the potential energy surface. There is however another difference between the two models at the level of the migration mechanism itself. This is specially evident by comparison of Figs. 3 and 4, namely the SR jump is clearly the lowest energy in Mo and this precludes multiple jumps along $\langle 111 \rangle$ directions. The preference for SR jumps is even greater for potentials built within the Embedded Defect (ED) model [21,7,12], a semiempirical development that includes angular contributions to the energy. Other potentials in the literature accounting for bond effects [22] but built on different grounds than ED obtain the same result. These findings together with the general consensus that in bcc transition metals bond directionality should arise from the *d* electrons, leads one to conclude that the fast 1D migration of small interstitial clusters found in MD simulations of collisional cascades [4] using spherical potentials, may be hindered.

Acknowledgements

References

[1] B.D. Wirth, G.R. Odette, D. Maroudas, G.E. Lucas, J. Nucl. Mater 224 (1997) 185.

[2] YuN. Osetsky, A. Serra, Def. Diff. Forum 143–147 (1997) 155.

[3] R. Pasianot, A.M. Monti, J. Nucl. Mater. 264 (1998) 198.

[4] D.J. Bacon, A.F. Calder, F. Gao, J. Nucl. Mater. 251 (1997) 1.

[5] G.H. Vineyard, J. Phys. Chem. Solids 3 (1957) 121.

[6] G. Simonelli, R. Pasianot, E.J. Savino, Phys. Stat. Sol. (b) 191 (1995) 249.

[7] G. Simonelli, R. Pasianot, E.J. Savino, Phys. Rev. B 55 (1997) 5570.

[8] P. Ehrhart, K. Robrock, H. Schober, in: R.A. Johnson, A.N. Orlov (Eds.), Physics of Radiation Effects in Crystals, Elsevier, Amsterdam, 1986, p. 3.

[9] P. Ehrhart, B. Schönfeld, in: V. Takamura, J. Doyama, M. Kiritani (Eds.), Proceedings of Yamada Conference on Point Defects and Defect Interactions in Metals, Tokyo University, 1982, p. 47.

[10] P. Ehrhart, J. Nucl. Mater 69&70 (1978) 200.

[11] M. Norgett, R.C. Perrin, E.J. Savino, J. Phys. F 2 (1972) L73.

[12] G. Simonelli, PhD thesis, Universidad Nacional de Buenos Aires, 1998.

[13] R. Fletcher, C.M. Reeves, Comput. J. 7 (1964) 149.

[14] M.S. Daw, S.M. Folies, M.I. Baskes, Dynamo code version 5.2, Sandia National Laboratory (1985).

[15] M.W. Guinan, R.N. Stuart, R.J. Borg, Phys. Rev. B 15 (1977) 699.

[16] B.J. Whiting, D.J. Bacon, MRS Symp. Proc. 439 (1997) 389.

[17] G.J. Ackland, S.J. Wooding, D.J. Bacon, Philos. Mag. A 71 (1995) 553.

[18] H. Ullmaier, ed., Atomic Defects in Metals, Landolt-Börnstein series, vol. III/25, Springer, Berlin, 1991.

[19] R. Thetford, in: R.M. Nieminen, M.J. Puska, M.J. Maninen (Eds.), Many-Atom Interactions in Solids, Springer, Berlin, 1990, p. 176.

[20] S. Sastry, P.G. Debenedetti, F.H. Stillinger, Nature 393 (1998) 554.

[21] R. Pasianot, D. Farkas, E.J. Savino, Phys. Rev. B 43 (1991) 6952.

[22] W. Xu, J.A. Moriarty, Phys. Rev. B 54 (1996) 6941.